

Effect of Annealing on the Superconducting and Structural Properties of Aerosol-Deposited Bi-2223 Films

Marina Mendoza, Shunsuke Omori, Kenji Sakai, Shinzo Yoshikado, Yuuki Sato, Ryo Matsumoto, Yoshihiko Takano

Abstract— $\text{Bi}_2\text{Sr}_2\text{Ca}_2\text{Cu}_3\text{O}_x$ (Bi-2223) is a high- T_c cuprate with potential for high-current applications, yet thin-film fabrication remains challenging due to multi-step, high-temperature processes. In this study, Bi-2223 films were fabricated on Ag substrates using aerosol deposition (AD), a room-temperature process that enables the rapid formation of dense ceramic films. The influence of multistep annealing on their structural and superconducting properties was systematically investigated. X-ray diffraction (XRD) revealed that as-deposited films retained Bi-2223 peaks with weak orientation, while annealing improved the c -axis texture but also induced partial Bi-2212 formation. Scanning electron microscopy (SEM) showed a transition from dense particle-boundary microstructures to porous, plate-like grains with local compositional inhomogeneity. Electrical resistance measurements confirmed superconducting transitions whose sharpness and T_c were correlated with phase and texture. These results demonstrate the tunability of AD-grown Bi-2223 films by annealing, underscoring the method's potential as a rapid alternative to conventional film processes for superconducting device applications.

Index Terms—Bi-2223, aerosol deposition, thick films, annealing, high- T_c cuprates.

I. INTRODUCTION

BISMUTH-strontium-calcium-copper-oxide (BSCCO) cuprates remain central to high-temperature superconductor (HTS) research for power technologies because they sustain large current densities near the boiling point of liquid nitrogen [1]–[4]. Within this family, the $n = 3$ phase $\text{Bi}_2\text{Sr}_2\text{Ca}_2\text{Cu}_3\text{O}_x$ (Bi-2223) is valued for its relatively high critical temperature at around 110 K and use in conductor architectures, although fabrication is constrained by a narrow phase-stability window and competition from lower- n phases such as Bi-2212 during thermal processing [5]–[7]. These materials considerations make process design that includes precursor chemistry, thermal history, and post-deposition annealing decisive for achieving ideal phase fraction, texture, and connectivity [8]–[12].

Aerosol deposition (AD) is a solid-state film fabrication technique in which fine ceramic particles are accelerated in a carrier gas toward a substrate under low pressure and consolidate at or near room temperature by room-temperature impact consolidation (RTIC) which is the fragmentation, plastic deformation, and mechanical bonding without sintering [13], [14]. Foundational and review works have established the process physics, equipment, and parameter space, and have demonstrated dense, adherent ceramic layers from sub-micron to multi-micron thicknesses [15]–[17].

Because AD can form dense films on metals and temperature-sensitive substrates without high thermal condi-

tions, it is used in electronics and functional ceramics, including dielectric and piezoelectric thick films such as BaTiO_3 , PZT, and PMN-PT, and in energy-storage layers, often with favorable microstructure and properties after modest post-treatments [18]–[21]. In contrast, applications of AD to cuprate superconductors remain comparatively few in the archival literature; most film reports on BSCCO have used spray pyrolysis, chemical solution routes, sputtering, or pulsed-laser deposition, so process–structure–property relations specific to AD-derived Bi-2223 thick films, including the correlation among post-deposition annealing, phase composition between Bi-2223 and Bi-2212, c -axis texture, microstructure, and transport, are not yet well resolved [11], [22]–[24].

II. EXPERIMENTAL METHODS

A. Precursor Preparation

Bi_2O_3 (99.999%), PbO (99%), SrO (97%), CaO (99.9%), and CuO (99.99%) were weighed to the nominal compositional ratio of $\text{Bi}_{1.75}\text{Pb}_{0.35}\text{Sr}_{1.9}\text{Ca}_{2.1}\text{Cu}_3$ and homogenized by mortar and pestle. The powder was uniaxially pressed into 20 mm pellets at 40 MPa under vacuum for 5 min, placed on a Pt plate in an alumina box, and heat treated in air. The pellets were then calcined at 840 °C, re-pulverized, re-pelletized, and sintered at 870 °C for 8 h. A multi-step anneal at 850 °C for 24 h followed by 820 °C for 24 h was then applied.

The annealed bulk was pre-ground for 30 min with a mortar and pestle. 10 g of powder was wet-milled (Pulverisette 7, Fritsch) with 50 g of 3 mm ZrO_2 balls and 6 g acetone as a wet medium combined in a 45 mL Al_2O_3 pot at 600 rpm in four cycles of 10 min milling and 10 min rest, then dried at 75 °C for 2 h.

B. Aerosol Deposition (AD) Process

Aerosol deposition was performed in a low-pressure system comprising an aerosol chamber, a deposition chamber, carrier-gas mass flow controller, and a nozzle-substrate stage with programmable motion. Vacuum was provided by a rotary pump (VD301, ULVAC) in series with a mechanical booster pump (PMB001CM, ULVAC), and a dust filter was installed upstream of the booster pump. A schematic of the system is shown in Fig. 1.

Powder aerosolization was aided by a rotary vibrator (NCR 3, NetterVibration) around the aerosol chamber. The vibration intensity was adjusted through the air pressure supplied from an air compressor (SLP-07E, Anest Iwata). For each run, 10 g of milled Bi-2223 powder and 10 g of soda-lime glass beads ($\varnothing = 0.1$ mm) were loaded into the aerosol chamber.

TABLE I
AEROSOL DEPOSITION PARAMETERS

Parameter	Setting / Range
Carrier-gas flow rate	8–12 L/min
Substrate temperature	200 °C
Nozzle outlet	0.3 × 5 mm ²
Nozzle–substrate distance	10 mm
Scan area	≈ 5 × 20 mm ²
Scan rate	20–100 μm/s

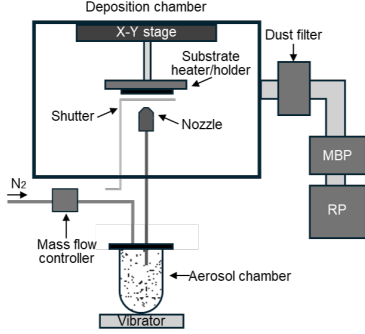


Fig. 1. Aerosol deposition system schematic.

TABLE II
SPECIMEN IDENTIFIERS AND INITIAL ANNEALING TEMPERATURE T_a .

Thickness (μm)	Sample	T_a (°C)
45	1A	860
	1B	865
141	2A	855
	2B	860

Carrier-gas inflow was regulated by a mass-flow controller; the chamber included a gas inlet with an auxiliary port for powder mixing. Inside the deposition chamber, a converging nozzle connected to the aerosol chamber directed the aerosol toward the substrate mounted on a motorized x - y stage capable of bidirectional or unidirectional motion along programmed scan paths. Before deposition, the chambers were evacuated to a base pressure of approximately 10 Pa; opening the N₂ line to generate and transport the aerosol raised the working pressure above the base level. A shutter between nozzle and substrate enabled clean start/stop.

Silver substrates were prepared from annealed Ag sheet (99.99%), cut to 20 × 20 mm² and annealed in air at 880 °C for 1 h prior to mounting on the heated stage. Film consolidation occurred by RTIC at the substrate surface during scanning over the defined area. Thickness was controlled primarily by the number of passes at a set scan rate.

C. Post-deposition Annealing

Following aerosol deposition, films were annealed in air using a multi-step schedule. An initial anneal at a specimen-specific temperature T_a was applied for 3 h, after which all samples underwent the same sequence of 840 °C for 3 h, dwell for 8 h, and 820 °C for 3 h. In this study, T_a was selected from 855–865 °C depending on the specimen. The thermal schedule is summarized in Table II.

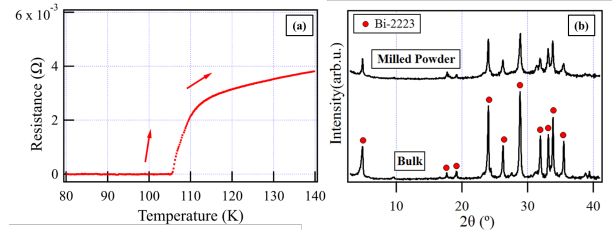


Fig. 2. (a) Bulk R - T curve ($T_c \approx 105$ K) and (b) XRD patterns of bulk precursor and milled powder.

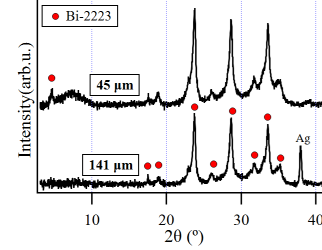


Fig. 3. XRD pattern of the as-deposited Bi-2223 films.

D. Characterization Methods

Phase analysis was performed by X-ray diffraction (XRD; MultiFlex, Rigaku; X'Pert Pro MRD, PANalytical) using Cu K α radiation. Particle size distributions of precursor powders were measured by laser diffraction (Microtrac S3500, Nikkiso). Microstructure and elemental distribution were examined by scanning electron microscopy with energy-dispersive X-ray spectroscopy (SEM/EDX; JSM-7001F, JEOL) operated in backscattered electron (BSE) mode for compositional imaging. Film thickness was determined by stylus profilometry (Dektak 150, ULVAC). Electrical resistance was measured by a standard four-probe method using a KEITHLEY 2400 current source and KEITHLEY 2182A nanovoltmeter with 1.4 mm probe spacing.

III. RESULTS AND DISCUSSION

A. Precursor Characterization

The Bi-2223 bulk precursor was verified by XRD prior to milling and exhibited a superconducting transition near 105 K in Fig. 2(a) which is used as a reference T_c for this composition. The milled powder retained Bi-2223 reflections with noticeable peak broadening relative to the bulk, indicating reduced crystallite size in Fig. 2(b) [25]. Laser diffraction after four milling cycles gave a median particle size of approximately 1.6 μm, suitable for aerosol deposition.

B. As-deposited Film

The as-deposited films showed the primary Bi-2223 peaks consistent with the precursor powder, indicating that the phase composition was largely retained after deposition as shown in Fig. 3. The peaks were broadened and less intense than those of the powder, reflecting reduced crystallinity mainly attributed to the nanoscale crystallite size and the absence of preferred

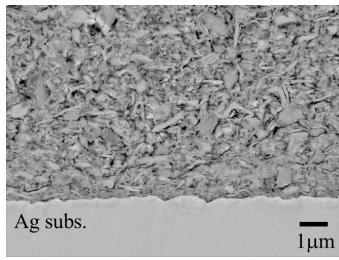


Fig. 4. Cross-sectional SEM-BSE image of the as-deposited film.

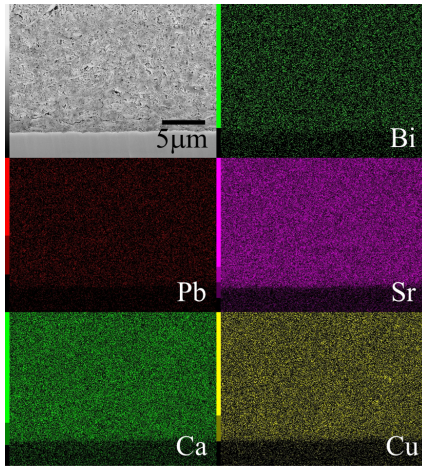


Fig. 5. EDX elemental mapping of Bi, Pb, Sr, Ca, and Cu in as-deposited film.

orientation which is typical of RTIC [26]. Film thickness did not notably influence the diffraction pattern.

SEM in Fig. 4 showed a dense surface of compacted particles with limited porosity. EDX mapping in Fig. 5 confirmed uniform elemental distribution of Bi, Pb, Sr, Ca, and Cu. The lack of evident grain coalescence suggests that post-deposition annealing is necessary to enhance crystallinity and interparticle connectivity.

C. Annealed Films

XRD patterns of the annealed films in Fig. 6 confirmed Bi-2223 as the main phase with the appearance of peaks associated with Bi-2212. The Bi-2223 reflections became sharper and more intense after annealing, particularly for the (00 l) peaks at characteristic 2θ positions, indicating improved crystallinity and preferential c -axis alignment. However, the emergence of Bi-2212 implies that the thermal treatment exceeded the narrow stability range of Bi-2223 under oxygen-rich conditions [27].

SEM images in Fig. 7 revealed the microstructural evolution toward coarser and more textured grains. All films exhibited enhanced grain definition, showing a densely packed, layered morphology composed of plate-like grains. However, pores and secondary phases became increasingly evident after annealing. The Bi-2223 (gray) and Bi-2212 (lighter gray) regions appeared to be intergrown, forming lamellar domains in which both phases coexist. This intergrowth is commonly observed in BSCCO systems due to the close lattice match and similar

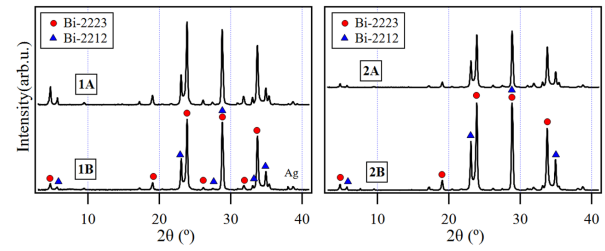


Fig. 6. XRD patterns of annealed films (Samples 1A, 1B, 2A, 2B).

layered crystal structures of the two phases [6]. Sample 2A, initially annealed at 855 °C, had fewer pores compared to Sample 1A and 2A but a crack extending from the surface to the substrate was observed.

EDX mapping in Fig. 8 confirmed that the matrix regions corresponded to Bi-2223/2212, while darker patches enriched in Ca, Cu, and Sr indicated the formation of Ca–Cu–O and Sr–Ca–Cu–O inclusions. These non-superconducting regions reduce effective connectivity and correlate with resistive behavior [28]–[30]. No evidence of Ag diffusion was detected at any post-annealing temperature. Combined with SEM and XRD results, the compositional analysis confirms the coexistence of Bi-2212 and Bi-2223 in the annealed films. Although these techniques clarify the structural and compositional state of the films, they cannot quantify the relative superconducting contribution of each phase. Magnetic susceptibility and critical current density (J_c) measurements, as reported in prior BSCCO studies [1], [31], could further elucidate their respective roles. The influence of these microstructural features was directly reflected in the electrical response, as shown by the resistance–temperature (R – T) curves in Fig. 9. Samples 1A and 1B exhibited lower normal-state resistance with broad transitions: Sample 1A showed a single transition with zero resistance at 85 K, while Sample 1B displayed a two-step transition with onset at 100 K but failed to reach zero resistance even below 60 K. This broad transition behavior can be attributed to the intergranular coexistence of Bi-2212 and Bi-2223 phases, which form weakly coupled regions with different critical temperatures, resulting in inhomogeneous current paths [32]. In contrast, the thicker Samples 2A and 2B showed higher normal-state resistance. Sample 2A exhibited an incomplete transition with onset at 110 K and no zero resistance, whereas Sample 2B reached near-zero resistance around 100 K, with residual resistance persisting to approximately 90 K. The large crack observed in Sample 2A likely disrupted conductive grain pathways, while increased porosity and compositional inhomogeneity in the thicker films contributed to carrier scattering and weakened intergranular coupling [30], [33], [34].

Overall, annealing improved crystallinity and texture but also introduced pores, cracks, and secondary phases. These competing effects of Bi-2223 alignment, partial decomposition, and microstructural discontinuity govern the superconducting behavior of AD-grown Bi-2223 films. Precise control of annealing conditions is essential to stabilize Bi-2223 while maintaining grain connectivity and dense morphology.

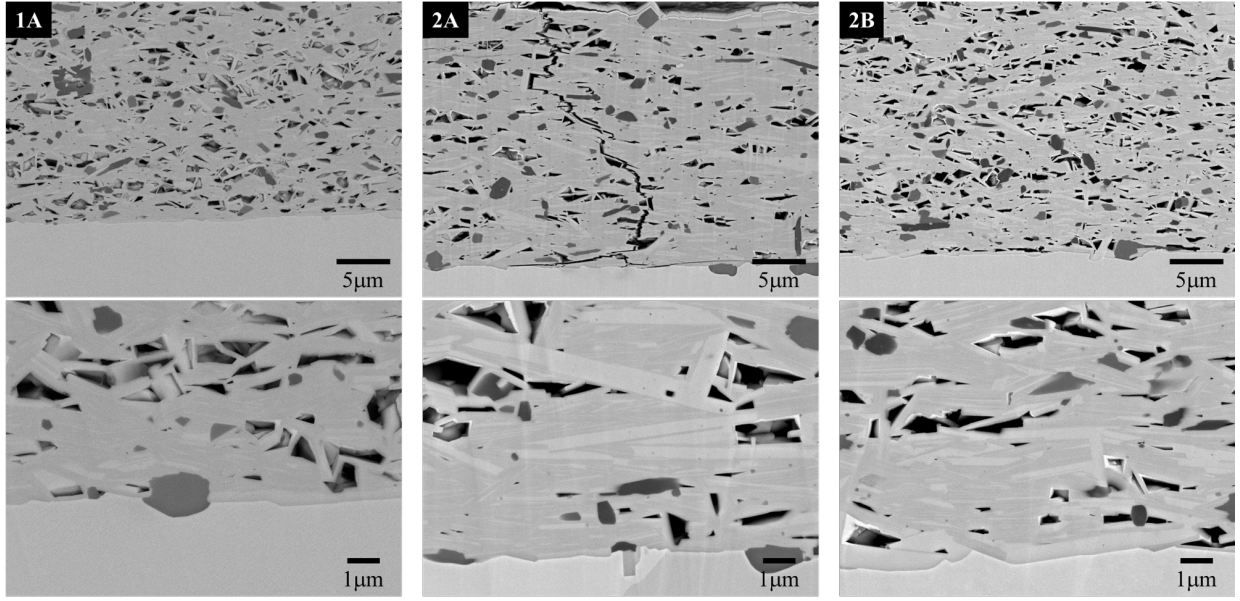


Fig. 7. Cross-sectional SEM-BSE images of annealed Bi-2223 films (Samples 1A, 2A, and 2B) showing compositional contrast and microstructural features at low (top) and high (bottom) magnifications.

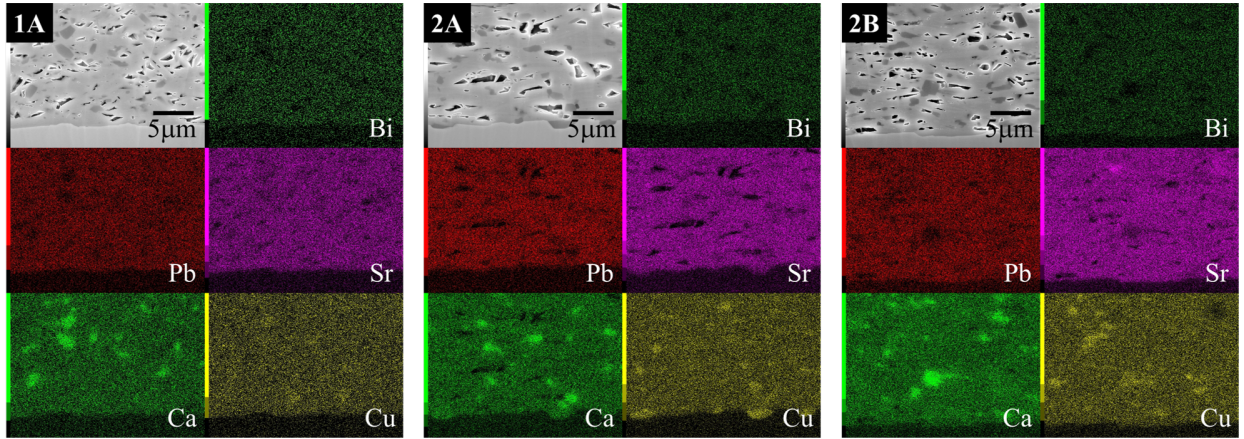


Fig. 8. EDX elemental mapping of Bi, Pb, Sr, Ca, and Cu in annealed films (Samples 1A, 2A, and 2B).

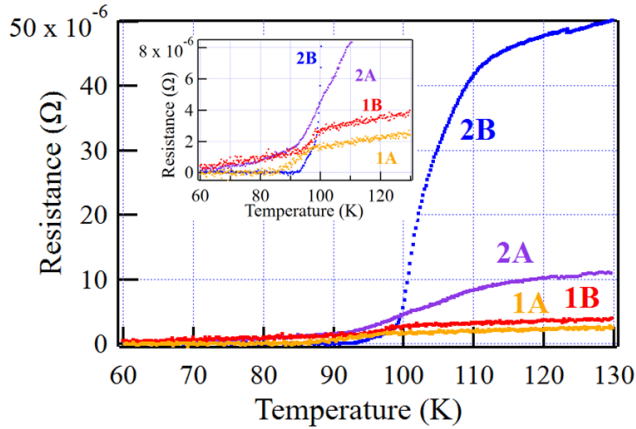


Fig. 9. Temperature dependence of resistance for annealed films.

IV. CONCLUSION

Bi-2223 thick films were successfully fabricated on Ag substrates by aerosol deposition and subsequently annealed to examine the effects of heat treatment on phase composition, texture, and superconducting behavior. Annealing enhanced crystallinity and c-axis alignment but also promoted partial Bi-2212 formation and introduced pores and cracks. These structural changes significantly influenced electrical transport, where improved texture competed with reduced connectivity caused by secondary phases and disrupted grain boundaries. Optimizing the annealing atmosphere, thermal schedule, and deposition conditions is crucial to suppress Bi-2212 and other non-superconducting phases, stabilize Bi-2223, and further advance aerosol deposition as a rapid route for high- T_c superconducting coatings.

REFERENCES

- [1] S. Abdelhaleem, M. O. Alziyadi, A. Alruwaili, M. J. Alawi, A. Alkabsh, and M. Shalaby, "BscCo high T_c -superconductor materials: strategies toward critical current density enhancement and future opportunities," *Appl. Phys. A*, vol. 131, no. 2, p. 151, 2025.
- [2] J. Shimoyama and T. Motoki, "Current status of high temperature superconducting materials and their various applications," *IEEE Trans. Electr. Electron. Eng.*, vol. 19, no. 3, pp. 292–304, 2024.
- [3] M. Kikuchi, N. Ayai, J. Fujikami, S. Kobayashi, K. Yamazaki, S. Yamade, T. Ishida, T. Kato, K. Hayashi, K. Sato *et al.*, "Progress in high performance di-bscCo wire," in *AIP Conf. Proc.*, vol. 986, no. 1. American Institute of Physics, 2008, pp. 407–415.
- [4] Y. L. Chen and R. Stevens, "2223 phase formation in bi (pb) sr ca cu o: I, the role of chemical composition," *J. Am. Ceram. Soc.*, vol. 75, no. 5, pp. 1142–1149, 1992.
- [5] O. V. Kharissova, E. M. Kopnin, V. V. Maltsev, N. I. Leonyuk, L. M. León-Rossano, I. Y. Pinus, and B. I. Kharisov, "Recent advances on bismuth-based 2223 and 2212 superconductors: synthesis, chemical properties, and principal applications," *Crit. Rev. Solid State Mater. Sci.*, vol. 39, no. 4, pp. 253–276, 2014.
- [6] A. Polasek, P. Majewski, E. T. Serra, F. Rizzo, and F. Aldinger, "Phase relations study on the melting and crystallization regions of the bi-2223 high temperature superconductor," *Mater. Res.*, vol. 7, pp. 393–408, 2004.
- [7] M. Yavuz, H. Maeda, L. Vance, H. K. Liu, and S. X. Dou, "Phase development and kinetics of high temperature bi-2223 phase," *J. Alloys Compd.*, vol. 281, no. 2, pp. 280–289, 1998.
- [8] U. Syamaprasad, M. Sarma, P. Guruswamy, V. P. Kumar, R. Ragini, K. Warriar, and A. Damodaran, "Effect of precursor phase assemblage on 2223 phase formation and jc in ag/(bi, pb)-2223 tapes," *Physica C*, vol. 297, no. 1–2, pp. 85–90, 1998.
- [9] X. Lu, A. Nagata, K. Watanabe, T. Nojima, K. Sugawara, S. Hanada, and S. Kamada, "Formation and texture of bi-2223 phase during sintering in high magnetic fields," *Physica C*, vol. 392, pp. 453–457, 2003.
- [10] S. S. Oh, T. Kubota, and K. Osamura, "Annealing temperature dependence of the superconducting properties of ag-sheathed bi-pb-sr-ca-cu-o tapes," *Physica C*, vol. 171, no. 3–4, pp. 265–270, 1990.
- [11] S. Takahira, Y. Ichino, and Y. Yoshida, "Fabrication of high jc (bi, pb) 2223 thin films by pld and post-annealing process," *Phys. Procedia*, vol. 65, pp. 153–156, 2015.
- [12] H. Ogawa, A. Kan, and M. Ohsashi, "Superconducting properties of zno-doped (bi, pb)-2223 thick film on ni and nio substrates prepared by spray deposition technique," *Physica C*, vol. 468, no. 6, pp. 447–452, 2008.
- [13] J. Akedo, "Aerosol deposition of ceramic thick films at room temperature: densification mechanism of ceramic layers," *J. Am. Ceram. Soc.*, vol. 89, no. 6, pp. 1834–1839, 2006.
- [14] D. Hanft, J. Exner, M. Schubert, T. Stöcker, P. Fuierer, and R. Moos, "An overview of the aerosol deposition method: Process fundamentals and new trends in materials applications," *J. Ceram. Sci. Technol.*, vol. 6, no. 3, pp. 147–182, 2015.
- [15] B. Xie, R. Hassan-Naji, and D. A. Hall, "Effects of process parameters on deposition behavior and mechanical properties of alumina coatings by aerosol deposition," *J. Am. Ceram. Soc.*, vol. 108, no. 2, p. e20169, 2025.
- [16] M. Schubert, M. Hahn, J. Exner, J. Kita, and R. Moos, "Effect of substrate hardness and surface roughness on the film formation of aerosol-deposited ceramic films," *Funct. Mater. Lett.*, vol. 10, no. 04, p. 1750045, 2017.
- [17] R. Saunders, S. D. Johnson, D. Schwer, E. A. Patterson, H. Ryou, and E. P. Gorzkowski, "A self-consistent scheme for understanding particle impact and adhesion in the aerosol deposition process," *J. Therm. Spray Technol.*, vol. 30, no. 3, pp. 523–541, 2021.
- [18] F. Zhuo, U. R. Eckstein, N. H. Khansur, C. Dietz, D. Urushihara, T. Asaka, K.-i. Kakimoto, K. G. Webber, X. Fang, and J. Rödel, "Temperature-induced changes of the electrical and mechanical properties of aerosol-deposited batf3 thick films for energy storage applications," *J. Am. Ceram. Soc.*, vol. 105, no. 6, pp. 4108–4121, 2022.
- [19] S. Baba, H. Tsuda, and J. Akedo, "Thickness dependence of electrical properties of pzt films deposited on metal substrates by laser-assisted aerosol deposition," *IEEE Trans. Ultrason. Ferroelectr. Freq. Control*, vol. 55, no. 5, pp. 1009–1016, 2008.
- [20] C.-T. Chen, S.-C. Lin, U. Trstenjak, M. Spreitzer, and W.-J. Wu, "Comparison of metal-based pzt and pmn-pt energy harvesters fabricated by aerosol deposition method," *Sensors*, vol. 21, no. 14, p. 4747, 2021.
- [21] M. Sadl, A. Lebar, J. Valentincic, and H. Ursic, "Flexible energy-storage ceramic thick-film structures with high flexural fatigue endurance," *ACS Appl. Energy Mater.*, vol. 5, no. 6, pp. 6896–6902, 2022.
- [22] J. Yoo, S. Kim, J.-W. Ko, and Y.-K. Kim, "The fabrication of fine and homogenous bi-2223 precursor powder by a spray pyrolysis process," *Supercond. Sci. Technol.*, vol. 17, no. 9, p. S538, 2004.
- [23] A. Matsumoto and H. Kitaguchi, "Critical current density enhancement of bi, pb-2223 thin film fabricated by rf sputtering and post-annealing processes," *Supercond. Sci. Technol.*, vol. 27, no. 1, p. 015002, 2013.
- [24] X. Lu, T. Wang, and Y. Qi, "Crystalline characteristics and superconducting properties of bi2212 thin films by pechini sol-gel method: effect of heating rate on the film growth," *J. Sol-Gel Sci. Technol.*, vol. 77, no. 1, pp. 100–108, 2016.
- [25] Y. Chen, L. Shao, G. Zhao, Q. Liu, Y. Huang, Z. Liu, L. Zhu, T. Wang, and B. Zheng, "Optimization for preparing bi1.68pb0.32sr1.75ca1.85cu2.85o10+y powders by wet ball milling," *Mater. Res. Express*, vol. 9, no. 6, p. 066002, 2022.
- [26] J. Akedo, "Room temperature impact consolidation (rtic) of fine ceramic powder by aerosol deposition method and applications to microdevices," *J. Therm. Spray Technol.*, vol. 17, no. 2, pp. 181–198, 2008.
- [27] J.-H. Ahn, H. Liu, and S. Dou, "Effect of oxygen partial pressure on processing conditions and phase transformation in ag/bi-2223 tapes," *Physica C*, vol. 351, no. 4, pp. 371–378, 2001.
- [28] L. G. Egeberg, *Structural Properties of Superconducting Bi-2223/Ag Tapes*. Risø National Laboratory, 2001.
- [29] X. Chen, Z. Han, M. Li, J. Meng, and Q. Liu, "Observation of the formation and growth of secondary phases in bi-2223/ag tapes," *Physica C*, vol. 391, no. 4, pp. 363–368, 2003.
- [30] R. Wu, Y. Yu, S. Jia, C. Zhou, O. Cojocar-Mirédin, and M. Wuttig, "Strong charge carrier scattering at grain boundaries of pbte caused by the collapse of metavalent bonding," *Nat. Commun.*, vol. 14, no. 1, p. 719, 2023.
- [31] A. Goyal, E. Specht, Z. Wang, D. M. Kroeger, J. Sutliff, J. Tkaczyk, J. Deluca, L. Masur, and G. Riley, "Dependence of critical current density on microstructure and processing of high- T_c superconductors," *J. Electron. Mater.*, vol. 23, no. 11, pp. 1191–1197, 1994.
- [32] G. Vadakkathillam, A. Sathyanarayana, E. Amaladass, K. Vinod, G. T. R. Pandian, and A. Mani, "Evolution of superconducting properties of coexistent bi-2212 and bi-2223 phases in bscCo," *Indian J. Pure Appl. Phys.*, vol. 59, pp. 391–397, 05 2021.
- [33] H. Hilgenkamp and J. Mannhart, "Grain boundaries in high- T_c superconductors," *Rev. Mod. Phys.*, vol. 74, no. 2, p. 485, 2002.
- [34] D. R. Clarke and M. DeGraef, "The effect of cracks on the superconducting transport current in thin films: The analogy with two-dimensional elasticity and plasticity," *J. Mater. Res.*, vol. 8, no. 7, pp. 1515–1532, 1993.